Draft version April 1, 2009
Preprint typeset using LaTeX style emulateapj v. 10/09/06

FINITE SOURCE EFFECTS IN MICROLENSING: A PRECISE, EASY TO IMPLEMENT, FAST AND NUMERICAL STABLE FORMALISM

C.-H. Lee[1], A. Riffeser[1], S. Seitz[1,2] and R. Bender[1,2]
1.University Observatory Munich, Scheinerstrasse 1, 81679 München, Germany and
2.Max Planck Institute for Extraterrestrial Physics, Giessenbachstrasse, 85748 Garching, Germany
Draft version April 1, 2009

ABSTRACT

The goal of this paper is to provide a numerically fast and stable description for the microlensing amplification of an extended source (either uniform or limb-darkened) that holds in any amplification regime. We show that our method of evaluating the amplification can be implemented into a light-curve fitting routine using the Levenberg-Marquardt algorithm. We compare the accuracy and computation times to previous methods that either work in the high-amplification regime only, or require special treatments due to the singularity of elliptic integrals.

In addition, we also provide the equations including finite lens effects in microlensing light curves. We apply our methods to the MACHO-1995-BLG-30 and the OGLE-2003-BLG-262 events and obtain results consistent to former studies. We derive an upper limit for the OGLE-2003-BLG-262 event lens size.

We conclude that our method allows to simultaneously search for point-source and finite-source microlensing events in future large area microlensing surveys in a fast manner.

Subject headings: dark matter — gravitational lensing — galaxies: halos — galaxies: individual (M31, NGC 224) — Galaxy: halo — galaxies: luminosity function, mass function

1. INTRODUCTION

In large area microlensing surveys, one has to search for microlensing signatures in billions of variable sources. This is straightforward to do and computationally inexpensive in the point-source approximation. One either fits a Paczyński light curve (Paczyński 1986), or, if appropriate, the Gould high-amplification approximation for point sources (Gould 1996). One major disadvantage of these point-source light curves is the infinite amplification for a lens exactly in front of the point source.

Gould (1994) extended Paczyński's light curve to finite sources which also avoids infinite amplifications. His equation describes the amplification as the two-dimensional integration of the Paczyński amplification over the circular source, assumed to have constant surface brightness.

Using the limiting form of Paczynski light curve under high amplification, Gould is able to factor out the two-dimensional integral into point source amplification times a much simpler integral. Meanwhile, Witt & Mao (1994) obtained the finite source amplification directly from the lens equation by comparing the area of the source and its lensed images. However, one needs to take care of the singular points for the elliptic integrals of the first and the third kind when using their formula.

In this paper we adopt the same strategy as Gould (1994), because in this way more general surface-brightness profiles for the sources (e.g. limb-darkened ones) can be taken into account straightforwardly. For the cases of a uniform disk we will also compare our results with Witt & Mao (1994).

The technical issue of the integration in the Gould extended source formalism can be carried out in several different ways. The two straightforward ones are to use polar coordinates and to choose the coordinate center either (1) at the source center or (2) at the lens center. Gould (1994) took the first choice. Riffeser *et al.* (2006) have shown for the very special case where the lens is positioned along the line of sight to the source that the integration can be solved very easily if the second option is chosen.

This leads us to choose the lens center as the coordinate center in general to benefit from the more simple integrand. We will show (in Section 2) that in this way the amplification of a uniform circular source is reduced to a one-dimensional integral and can be computed numerically fast and stable by using the composite Simpson's rule. A limb-darkened source is treated in Section 3. The two-dimensional integral can be solved numerically again in a fast and stable fashion, and light-curve fits for limb-darekened profiles can be obtained with the Levenberg-Marquardt algorithm (see Press *et al.* 2007) with less than 100 steps. We also allow for finite lens sizes in Section 4. As a test example, we apply our fitting methods to a MACHO (Alcock et al. 1992) event and an OGLE (The Optical Gravitational Lensing Experiment; Udalski et al. 1992) event in Section 5. We conclude in Section 6.

2. THE FINITE-SOURCE MICROLENSING EQUATION

We first introduce our notation. Let R_E be the Einstein radius of a point mass lens, and b be the impact parameter of a point source. Then one can write the amplification of the point source by the point mass lens as a function of the

Electronic address: chlee@usm.lmu.de

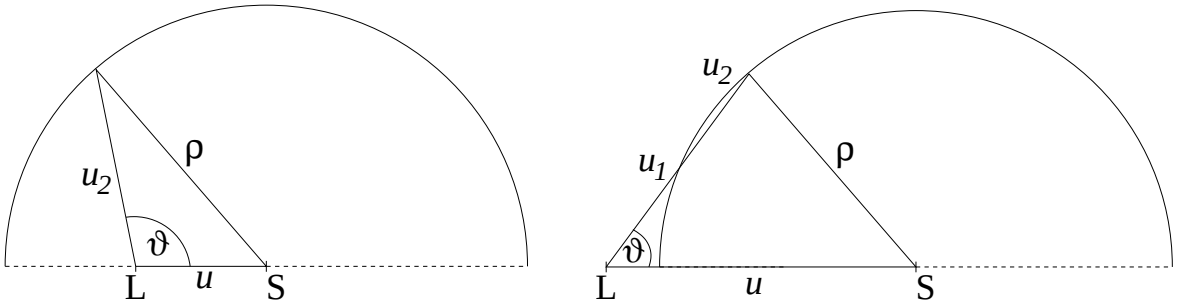

FIG. 1.— Geometric definitions. Left: source is overlapping the lens center. Right: lens is outside the source radius.

dimensionless impact parameter $u := b/R_E \equiv \theta/\theta_E$ as

$$A_{\rm PS}(u) = \frac{u^2+2}{u\sqrt{u^2+4}} \tag{1}$$

(Paczyński 1986).

If the source is extended one can obtain the lensed flux and the total amplification by integrating $A(u)$ over the source area, weighted by the surface-brightness profile of the source. We now derive the amplification for a circular source[1] with radius ρ ($\rho \equiv \frac{R_* D_{\rm ol}}{R_{\rm E} D_{\rm os}}$ is the projected source size in units of the Einstein radius R_E and R_* is the physical source size). The situation is sketched in Figure 1. There are two cases: either the center of the lens L (projected along the line of sight) is within the extended source centered at S (the left side of Figure 1) or the lens is outside the extended source (the right side of Figure 1), i.e., either $u \le \rho$ or $u > \rho$. One obtains the amplification of the extended uniform source by integrating the point-source amplification over the source area $\mathcal{A}_{\rm source}$:

$$A^*(u;\rho) = \frac{\int\limits_{\mathcal{A}_{\rm source}} A_{\rm PS}\, d\mathcal{A}}{\int\limits_{\mathcal{A}_{\rm source}} d\mathcal{A}} = \frac{1}{\pi\rho^2} \int\limits_{\mathcal{A}_{\rm source}} A_{\rm PS}\, d\mathcal{A}\ . \tag{2}$$

Using polar coordinates centered on the lens, one can write

$$A^*(u;\rho) = \tfrac{2}{\pi\rho^2} \int\limits_0^{\pi} \int\limits_{u_1(\vartheta)}^{u_2(\vartheta)} A_{\rm PS}(\tilde{u})\, \tilde{u}\, d\tilde{u}\, d\vartheta\ . \tag{3}$$

The integration boundaries u_1 and u_2 are

$$u_1(\vartheta) = \begin{cases} 0 & , u \le \rho \\ u\cos\vartheta - \sqrt{\rho^2 - u^2\sin^2\vartheta} & , u > \rho \wedge \vartheta \le \arcsin(\rho/u) \\ 0 & , u > \rho \wedge \vartheta > \arcsin(\rho/u) \end{cases}, \tag{4}$$

$$u_2(\vartheta) = \begin{cases} u\cos\vartheta + \sqrt{\rho^2 - u^2\sin^2\vartheta} & , u \le \rho \\ u\cos\vartheta + \sqrt{\rho^2 - u^2\sin^2\vartheta} & , u > \rho \wedge \vartheta \le \arcsin(\rho/u) \\ 0 & , u > \rho \wedge \vartheta > \arcsin(\rho/u) \end{cases}, \tag{5}$$

and so the amplification becomes

$$A^*(u;\rho) = \frac{1}{\pi\rho^2} \int\limits_0^{\pi} \left[u_2(\vartheta)\sqrt{u_2(\vartheta)^2+4} - u_1(\vartheta)\sqrt{u_1(\vartheta)^2+4} \right] d\vartheta\ , \tag{6}$$

which can be approximated numerically using the composite Simpson's rule with n(an even number) grids:

$$A^*(u;\rho) \approx \begin{cases} \frac{1}{\pi\rho^2}\frac{\pi}{2n}\left[\frac{(u+\rho)\sqrt{(u+\rho)^2+4} - (u-\rho)\sqrt{(u-\rho)^2+4}}{3} + \frac{2}{3}\sum\limits_{k=1}^{n-1} f\left(\frac{2k\pi}{2n}\right) + \frac{4}{3}\sum\limits_{k=1}^{n} f\left(\frac{(2k-1)\pi}{2n}\right) \right] & , u \le \rho \\ \frac{1}{\pi\rho^2}\frac{\arcsin(\rho/u)}{n}\left[\frac{(u+\rho)\sqrt{(u+\rho)^2+4} - (u-\rho)\sqrt{(u-\rho)^2+4}}{3} + \frac{2}{3}\sum\limits_{k=1}^{n/2-1} f\left(\frac{2k\arcsin(\rho/u)}{n}\right) + \frac{4}{3}\sum\limits_{k=1}^{n/2} f\left(\frac{(2k-1)\arcsin(\rho/u)}{n}\right) \right] & , u > \rho \end{cases}, \tag{7}$$

where $f(\vartheta) = [u_2(\vartheta)\sqrt{u_2(\vartheta)^2+4} - u_1(\vartheta)\sqrt{u_1(\vartheta)^2+4}]$. The upper limit of ϑ changes from $\frac{\pi}{2}$ to π when the lens crosses the edge of the source from outside to inside, thus we set a grid of $2n$ for $u \le \rho$ in order to have the same step size on both sides.

Gould (1994) argued that the finite-source effects are prominent only when the lens is very close to the source center ($u \ll 1$), and thus one can approximate Equation (1) by

[1] The reader is referred to Heyrovsky & Loeb (1997) for a more general case of elliptical source.

$$A_{\rm PS}(u) = \frac{u^2+2}{u\sqrt{u^2+4}} \approx u^{-1} \quad , u \ll 1 \ , \tag{8}$$

and the finite-source light curve can be obtained by solving elliptic integrals (see also Yoo *et al.* 2004; Cassan *et al.* 2006)

$$A^*{}_{\rm Gould}(u;\rho) \simeq A_{\rm PS}(u)\frac{4u}{\pi\rho}E\left(\vartheta_{\rm max}, \frac{u}{\rho}\right) \ , \tag{9}$$

where $E(\phi, k)$ is the elliptic integral of the second kind and $\vartheta_{\rm max}$ is defined as

$$\vartheta_{\rm max} = \begin{cases} \frac{\pi}{2} & , u \le \rho \\ \arcsin(\rho/u) & , u > \rho \end{cases} . \tag{10}$$

We now compare our method for $A^*(u;\rho)$ with previous ones, i.e. with Paczyński (1986), Gould (1994) and Witt & Mao (1994), and illustrate these comparisons in Figures 2 and 3.
Equation (9) and (10) allow a fast computation of finite-source light curves in the Gould approximation, which however is accurate only for a high-amplification event. This is shown in Figure 2, where for high amplifications (right panel) the Gould finite-source approximation (*gray*) is very close to the Witt & Mao (1994) light curve (displayed in *solid black*), but fairly off when the lens transits the source for low amplifications (left panel).

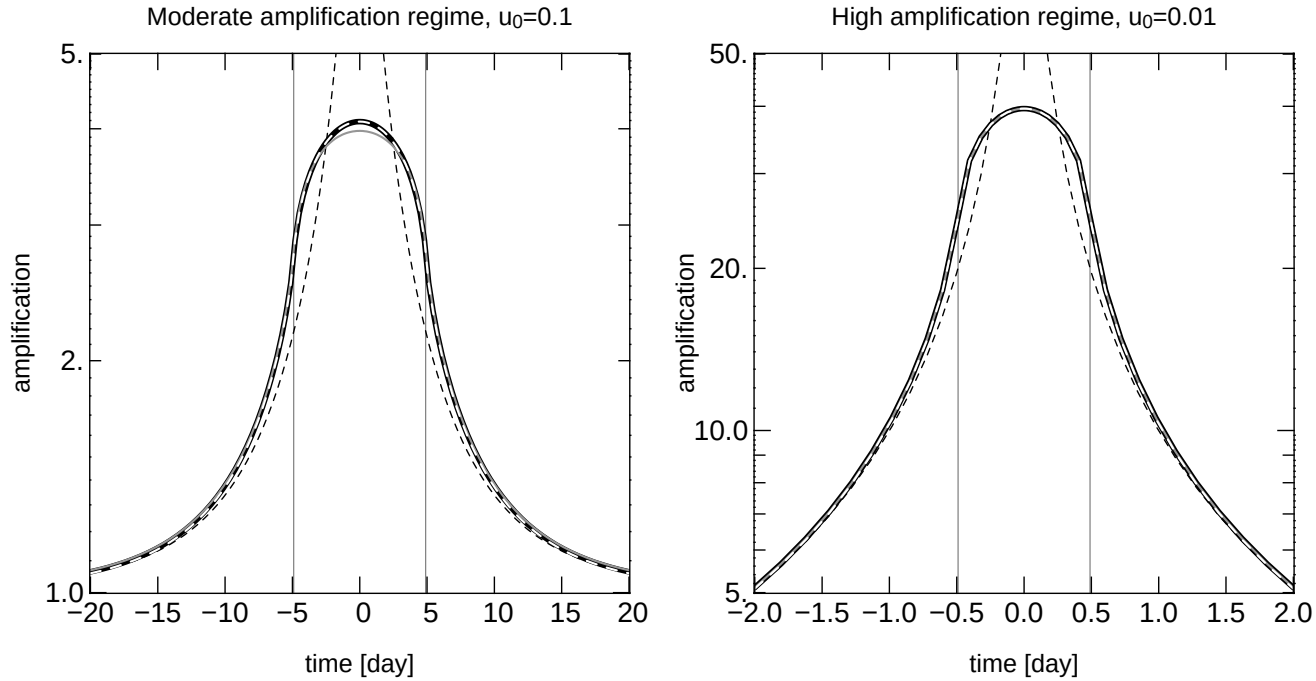

FIG. 2.— Comparison of finite-source light-curve approximations. Left: moderate-amplification regime with $t_E = 10$, $u_0 = 0.1$ and $\rho = 0.5$. Right: high-amplification regime with $t_E = 10$, $u_0 = 0.01$ and $\rho = 0.05$. In *dashed black* the Paczyński light curve for a point source, in *solid black* Witt & Mao light curve, in *gray* the approximation derived by Gould (1994) and in *dashed white* Equation (7) with $n = 10$. The vertical lines indicate the time when $u = \rho$. Our formula is as good as Gould (1994) in high-amplification regime and is better in the moderate-amplification regime.

Our formalism from Equation (6) and that of Witt & Mao (1994) both provide the exact light curves for uniform extended sources. In the Witt & Mao formalism one has to evaluate an elliptic integral which shows singularity when the impact parameter u is similar to the source size ρ. Witt & Mao therefore derived a separate solution for the case of $u = \rho$. This method is difficult to implement into numerical fitting routines in general, and particular cumbersome for those fast numerical fitting routines, where the partial derivatives have to be provided.

We therefore suggest to start from our exact formalism given in Equation (6) and estimate values for the integral using Equation (7) with $n = 10$. The comparison with results from higher values for $n = 500$ or the comparison with the Witt & Mao (1994) formalism – see the *gray* and *dash-dotted curves* in Figure 3 – shows that Equation (7) (with $n = 10$) provides a precise numerical estimate for the integral already. Another advantage of our formalism is that one can obtain the derivatives of Equation (6) with respect to source radius ρ and u in a straightforward manner (see Appendix A). This enables us to use fitting routines as, e.g., the Levenberg-Marquardt algorithm (see Press *et al.* 2007) which converge in this case in less than 100 iterations.

The approximation by Gould (1994) with $A_{\rm PS}(u)$ evaluated according to Equation (1) is actually valid for all u provided that $\rho \ll 1$, so it deviates from Equation (6) for larger source size. In fact, more than 80% (2548 out of

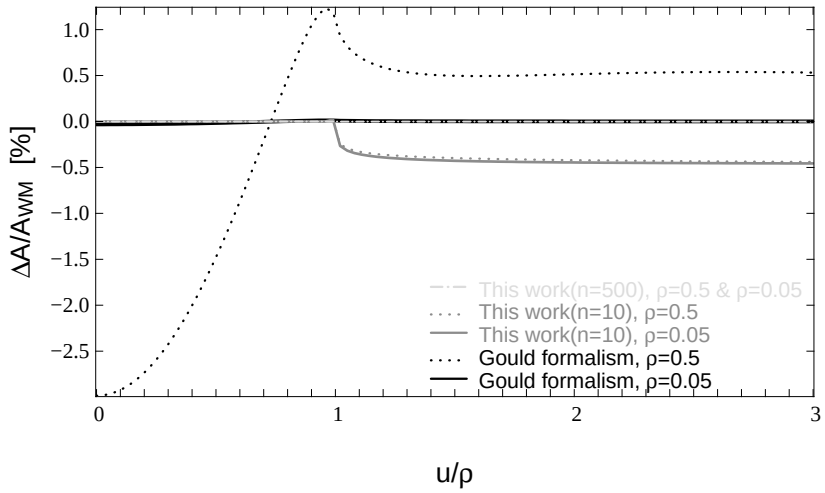

FIG. 3.— Percentage deviation in amplification compared to Witt & Mao formalism ($A_{\rm WM}$). The expression of Gould (1994) is valid for small source (*solid black*) but shows deviation $> 2.5\%$ for larger source (*dotted black*). Equation (7) with $n = 10$ shows a smaller deviation ($< 0.5\%$). Equation (7) with $n = 500$ for both source sizes are well overlapped with each other, so we show here only $\rho = 0.05$.

3153) of the microlensing events detected from the OGLE experiment[2] (Udalski 2003) have maximum amplification < 10 (see Figure 4). This highlights the necessity of a fast fitting routine for the moderate-amplification regime. We then compare the light-curve computation time of Equation (7) to Gould's formalism (see Figure 5). With $n = 10$, Equation (7) is about 38% faster then Gould's formalism when $u \leq \rho$ and is $> 55\%$ faster when $u > \rho$. Therefore, our $n = 10$ approximation turns out to be a practical fast fitting routine for both moderate- and high-amplification regimes.

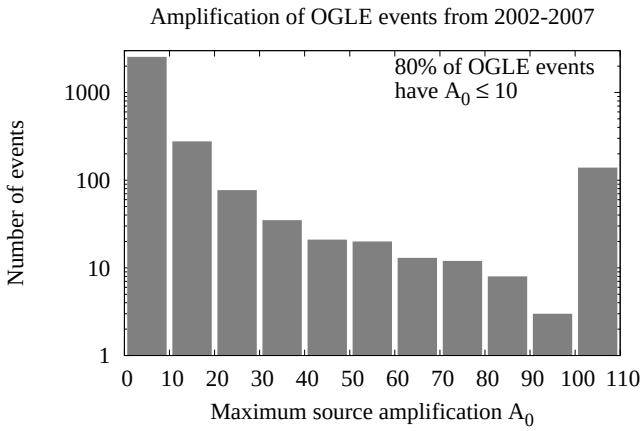

FIG. 4.— Maximum amplification of microlensing events detected by the OGLE experiment from 2002 to 2007. Most of the events ($> 80\%$) have maximum amplification < 10. Events with maximum amplification > 100 , which are categorized into interval 100-110 in this plot, are relatively rare ($< 4.4\%$).

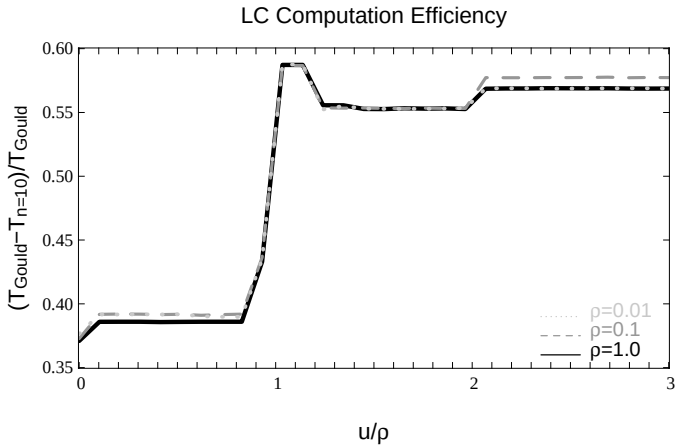

FIG. 5.— Light-curve computation efficiency. We compare light-curve computation time of Equation (7) with $n = 10$ to that of Gould's formalism for various source radii ($\rho = 0.01$, 0.1, and 1). The computation time for our approximation is comparable to the Gould formalism; it is about 38% faster when $u < \rho$ and is $> 55\%$ faster when $u > \rho$.

3. FINITE SOURCE WITH LIMB DARKENING

The next step towards a more precise microlensing light curve for extended sources is to account for limb darkening. Since the darkening is increasing towards the edges of the source, the limb darkening brings finite-source light curves closer to the Paczyński light curve which can be considered as the most extreme limb-darkening model with a delta function.

We use the one-parameter linear limb-darkening profile from Yoo *et al.* (2004) for the surface brightness of the source,

$$S(r/R_*, \Gamma) = \bar{S}\left[1 - \Gamma\left(1 - \frac{3}{2}\sqrt{1 - \left(\frac{r}{R_*}\right)^2}\right)\right] , \tag{11}$$

[2] http://ogle.astrouw.edu.pl/ogle3/ews/ews.html

where r is the distance to the source center.

Γ is the limb-darkening coefficient, and depends on the wavelength range used for the observations. $\bar{S}$ is the mean surface brightness of the source and defined as

$$\int_0^{2\pi}\int_0^{R_*} S(\tilde{r}/R_*,\Gamma)\tilde{r}d\tilde{r}d\vartheta = \pi {R_*}^2 \bar{S} \ . \tag{12}$$

We implemented the limb-darkening effects in our finite-source light curve as follows:

$$\begin{aligned} A^*{}_{\rm LD}(u;\rho) &= \frac{2}{\pi\rho^2\bar{S}}\int_0^{\pi}\int_{u_1(\vartheta)}^{u_2(\vartheta)} A_{\rm PS}(\tilde{u})\, S(r/R_*,\Gamma)\,\tilde{u}d\tilde{u}\,d\vartheta \\ &= \frac{2}{\pi\rho^2}\int_0^{\pi}\int_{u_1(\vartheta)}^{u_2(\vartheta)} \frac{\tilde{u}^2+2}{\sqrt{\tilde{u}^2+4}}\left[1-\Gamma\left(1-\frac{3}{2}\sqrt{1-\frac{\tilde{u}^2-2u\tilde{u}\cos\vartheta+u^2}{\rho^2}}\right)\right] d\tilde{u}\,d\vartheta \ . \end{aligned} \tag{13}$$

Equation (13) is still a double integral over $\tilde{u}$ and ϑ. But even here the divergent part cancels, and the function is numerically stable and can be evaluated using a small grid. The limb-darkening effects under moderate-amplification regime is shown in Figure 6.

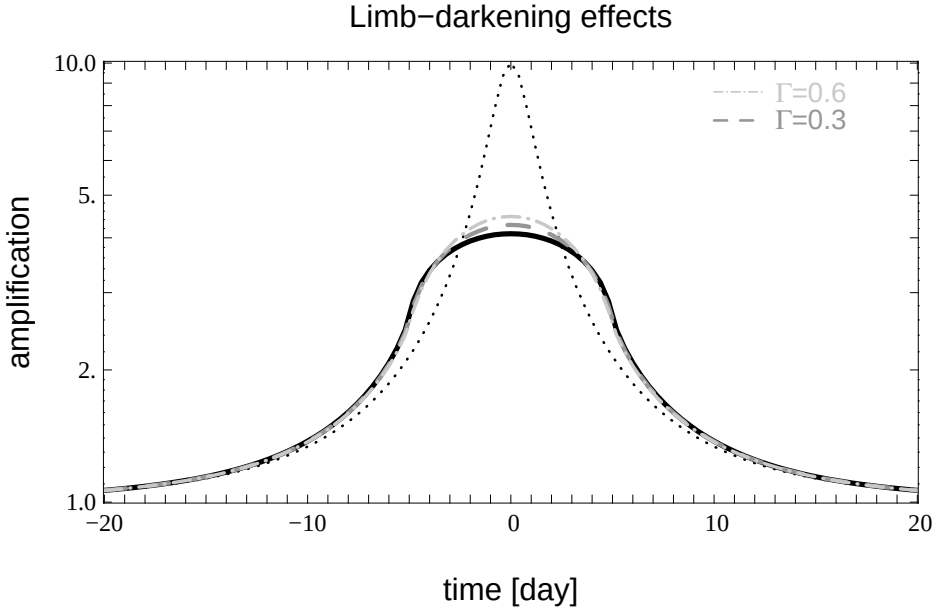

FIG. 6.— Limb-darkening effects on the finite-source light curve in the moderate-amplification regime. In *dotted black* we show the Paczyński light curve for a point source with $t_E = 10$ and $u_0 = 0.1$. In *solid black*, we show the finite-source light curve for a uniform source with a projected source size of $\rho = 0.5$. In *dashed line* and *dash-dotted line*, we plot the limb-darkened finite-source light curves with $\Gamma = 0.3$ and 0.6. Increasing Γ enhances the limb-darkening effects thus brings the finite-source light curve closer to Paczyńsky's formalism.

4. FINITE-SOURCE EQUATION WITH FINITE LENS

Given a finite-size lens, one can always find a time interval when the lens obscures the inner (and the outer, depending on the lens size) lensed image in the early rising stage and in the final declining stage of the light curve. In the following, we investigate how large this effect is depending on the lens size.

Agol (2002) derived the lens-modified amplification by calculating how much area is unobscured by the lens in the image plane. One has to solve for the image position by inverting the lens equation and one has to evaluate the image area from the image boundary using Stokes' theorem. Depending on the source and lens radii, there are 7 different cases for the inner image and 6 cases for the outer image to be considered if one follows the derivation of Agol.

Here we show that the finite lens amplification of a finite source again can be much more easily evaluated if one uses the polar coordinates $\tilde{u}$ and ϑ again. First, we consider a lens with physical radius $R_{\rm lens}$ transiting the surface of the source. The light emitted at a given point from the source follows the lens equation

$$\frac{b}{R_E} = \frac{b_\pm}{R_E} - \frac{R_E}{b_\pm} \ , \tag{14}$$

which gives the position of the two images in the lens plane (recall $u := \frac{b}{R_E}$)

$$\frac{b_\pm}{R_E} = \frac{u \pm \sqrt{u^2+4}}{2} \tag{15}$$

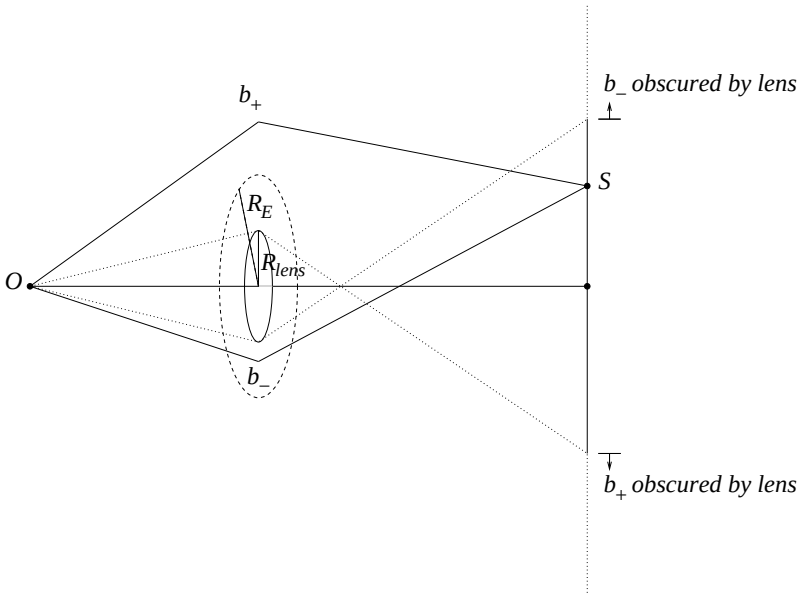

FIG. 7.— Image obscuration by a finite lens with radius $R_{lens} = 0.5R_E$.

with amplifications

$$A_{\pm}(u) = \frac{u^2+2}{2u\sqrt{u^2+4}} \pm \frac{1}{2} \ . \tag{16}$$

Here, $\frac{b_+}{R_E}$ denotes the outer image, and $\frac{b_-}{R_E}$ denotes the inner image in units of the Einstein radius. The sum of $A_+(u)$ and $A_-(u)$ gives the Paczyński light curve.

An image is unobscured if $-\frac{b_-}{R_E} > \rho_{\rm lens}$ or $\frac{b_+}{R_E} > \rho_{\rm lens}$ holds, where $\rho_{\rm lens} \equiv \frac{R_{\rm lens}}{R_{\rm E}}$ is the lens radius in units of the Einstein radius. Following this criterium and Figure 7, there exists an upper limit for $\frac{b_-}{R_E} < -\rho_{\rm lens}$ and a lower limit for $\frac{b_+}{R_E} > \rho_{\rm lens}$ to be unobscured by the lens. Therefore, we only need to consider these two limitations when integrating the amplification in Equation (3):

$$\begin{aligned} A^*{}_{\rm FL}(u;\rho) &= \tfrac{2}{\pi\rho^2} \int_0^{\pi} \int_{u_1(\vartheta)}^{u_2(\vartheta)} \left[A_+(\tilde{u})\Theta\left(\tfrac{b_+}{R_E} - \rho_{\rm lens}\right) + A_-(\tilde{u})\Theta\left(-\tfrac{b_-}{R_E} - \rho_{\rm lens}\right)\right] \tilde{u}\, d\tilde{u}\, d\vartheta \\ &= \tfrac{1}{\pi\rho^2} \int_0^{\pi} \left[\left(\tfrac{\tilde{u}}{2}\sqrt{\tilde{u}^2+4} + \tfrac{\tilde{u}^2}{2}\right)\Big|_{\max\left[u_1(\vartheta), \rho_{\rm lens} - \frac{1}{\rho_{\rm lens}}\right]}^{u_2(\vartheta)} + \left(\tfrac{\tilde{u}}{2}\sqrt{\tilde{u}^2+4} - \tfrac{\tilde{u}^2}{2}\right)\Big|_{u_1(\vartheta)}^{\min\left[u_2(\vartheta), -\rho_{\rm lens} + \frac{1}{\rho_{\rm lens}}\right]} \right] d\vartheta \ , \end{aligned} \tag{17}$$

where $\Theta(x)$ defines the Heaviside step function.

Combining Equation (13) and Equation (17) fully considers a limb-darkened source and a finite lens:

$$A^*{}_{\rm LD\&FL}(u;\rho) = \frac{2}{\pi\rho^2} \int_0^{\pi} \int_{u_1(\vartheta)}^{u_2(\vartheta)} \left[A_+(\tilde{u})\Theta\left(\frac{b_+}{R_E} - \rho_{\rm lens}\right) + A_-(\tilde{u})\Theta\left(-\frac{b_-}{R_E} - \rho_{\rm lens}\right)\right] S(r/R_*, \Gamma)\tilde{u}\, d\tilde{u}\, d\vartheta \ . \tag{18}$$

5. RESULTS

When we implemented the finite-source fitting using the Levenberg-Marquardt algorithm, we recognized that a good set of initial values is needed to bring the algorithm to convergence. Fitting a Paczyński light curve to derive these initial values for the finite-source fitting leads to very good results. The algorithm is stable and for an initial value of $\rho = 0.1$ it converges within 100 iterations.

Alcock *et al.* (1997) were able to measure a microlensing light curve with finite-source effects in MACHO-1995-BLG-30. We extracted the data points from their paper and applied our finite-source fitting algorithms to them. Fitting Equation (7) with $n = 10$ to the data yields a perfect agreement (see Table 1 and Figure 8) with the parameters given in Table 2 of Alcock *et al.* (1997):

Alcock *et al.* (1997) then obtained the limb darkening coefficients of MACHO-1995-BLG-30 utilizing spectroscopic information. However, Heyrovský (2003) argued that the surface-brightness profile of this event can not be fully recovered due to its intrinsic complex variability. Therefore, we tested our limb-darkening fitting routine to another limb-darkened finite-source event OGLE-2003-BLG-262. Our results are shown in Table 2, Figure 9 and Figure 10 in comparison with Yoo *et al.* (2004).

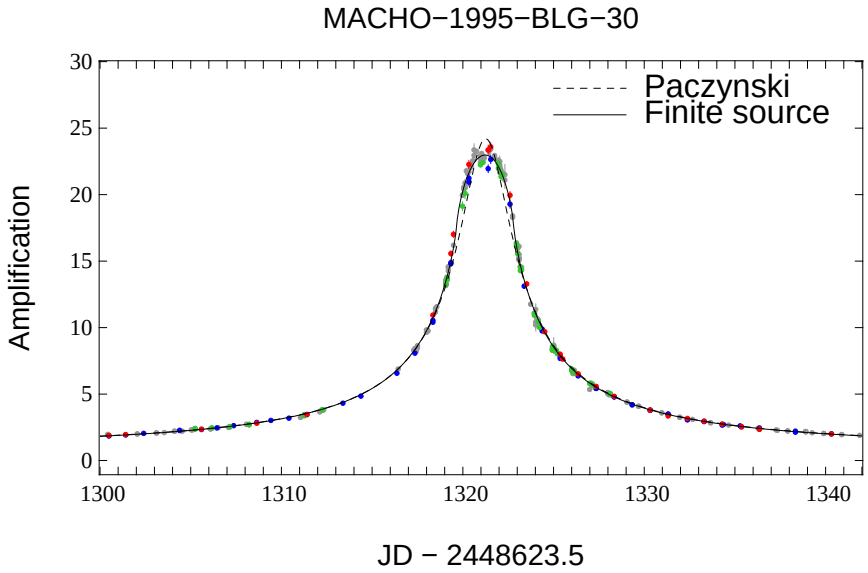

FIG. 8.— Finite-source light-curve fits for MACHO-1995-BLG-30 assuming a uniform source. Data points in R are from MACHO (*red*), CTIO, UTSO, WISE, and MJUO (*gray*) and V are from MACHO (*blue*) and UTSO (*green*). The *dashed line* shows the light curve for a point-source model. The best-fitting finite-source light-curve parameters are displayed in Table 1

TABLE 1
LIGHT-CURVE PARAMETERS FOR MACHO-1995-BLG-30

Fit	$A_{\rm PS}(u)$ (this work)	$A^*(u;\rho)$ (this work)	Alcock *et al.* (1997), Table 2[a]
t_0	1321.260 ± 0.002	1321.235 ± 0.002	1321.2(1)
t_E	34.41 ± 0.02	34.25 ± 0.02	33.68(1)
u_0	0.04133 ± 0.00004	0.05569 ± 0.00006	0.05579(1)
ρ	–	0.0722 ± 0.0001	0.07335(1)

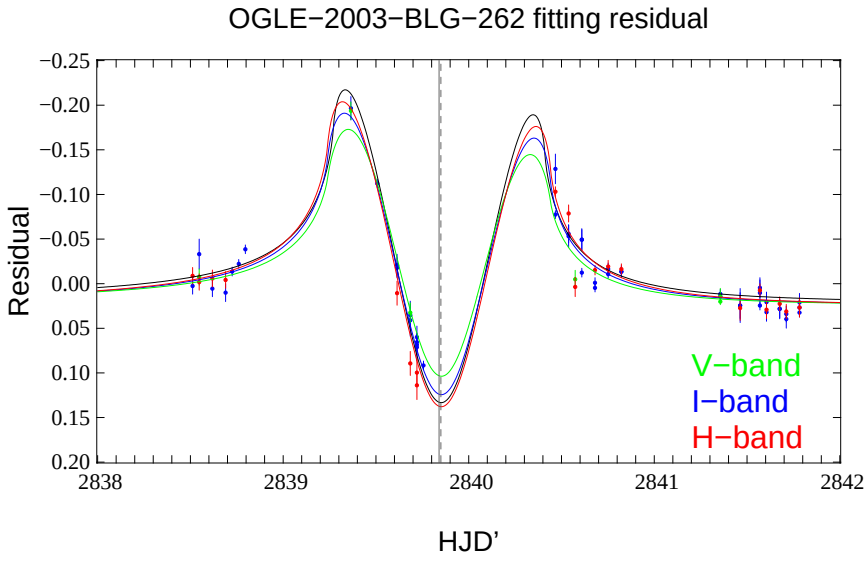

FIG. 9.— Residuals of the observed light curve relative to the best-fitted point-source light curve. The *solid black* curve shows the light curve of an extended source with uniform surface brightness. The *solid blue*, *solid red*, and *solid green* curves are extended source models incorporating limb darkening in V, I and H bands with $(\Gamma_V, \Gamma_I, \Gamma_H) = (0.72, 0.44, 0.26)$. The vertical lines indicate t_0 for the best-fitted point-source (*solid*) and limb-darkened finite-source (*dashed*) model. For the light curves with the limb-darkened source we have left t_0 as a free parameter. The best-fitting value for t_0 slightly differs (see Table 2). This causes the asymmetric pattern of the residual relative to the Paczyński light curve.

Finally, we choose several lens sizes for the configuration of OGLE-2003-BLG-262 to investigate the influence of the finite lens effects on the microlensing light curve in Figure 10. The light curve is strongly altered only if the lens size is comparable to or larger than the Einstein radius.

When the lens size is smaller than $0.93R_E$, it only partially covers the outer image and the finite lens effects can be observed only at the very beginning of the rising and near the end of the declining stage of the lensing event. Therefore,

TABLE 2
Light-curve parameters for OGLE-2003-BLG-262.

Fit	$A_{\rm PS}(u)$	$A^*(u;\rho)$	$A^*_{\rm LD}(u;\rho)$
t_0	2839.852 ± 0.001	2839.838 ± 0.001	2839.8361 ± 0.001
t_E	12.83 ± 0.01	12.61 ± 0.01	12.559 ± 0.016
u_0	0.02877 ± 0.00008	0.0365 ± 0.0002	0.0361 ± 0.0002
ρ	–	0.0581 ± 0.0002	0.0598 ± 0.0002

Note. We fixed the limb-darkening coefficients at $(\Gamma_V, \Gamma_I, \Gamma_H) = (0.72, 0.44, 0.26)$

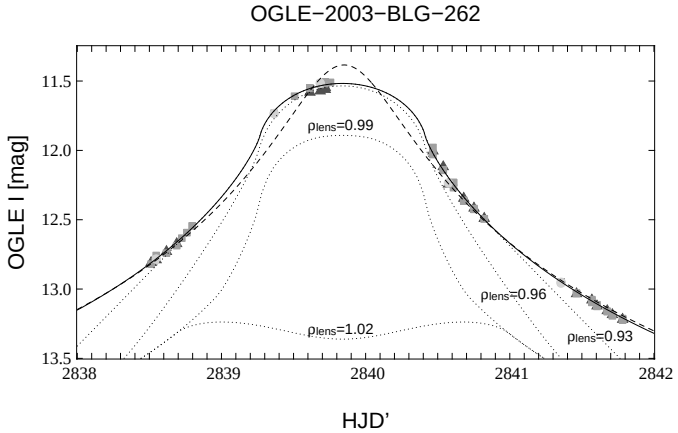

Fig. 10.— Finite-source and finite-lens light-curve fits for OGLE-2003-BLG-262. Data points are in I(square), V(circle), and H(triangle). The *dashed line* shows the light curve for a point source. The *solid line* shows the light curve for an extended source with uniform surface brightness. The *dotted lines* illustrate the effects of finite lens sizes on top of finite-source size for lens sizes of $\rho_{\rm lens} = 0.93$, 0.96, 0.99, and 1.02.

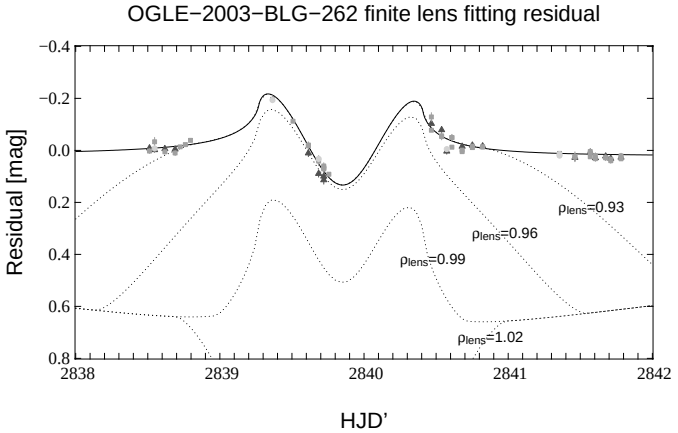

Fig. 11.— Fitting residual of various lens radius relative to the point-source model. Data points are in I(square), V(circle), and H(triangle). The *solid black line* shows the light curve for an extended source with uniform surface brightness. The *dotted lines* illustrate the effects of finite lens sizes on top of finite source size for lens sizes of $\rho_{\rm lens} = 0.93$, 0.96, 0.99, and 1.02. One sees that all these cases can be safely excluded.

we fitted various lens sizes up to $\rho_{\rm lens} = 1.1R_E$ using the full OGLE I-band data set. However, no improvement in χ^2 has been found by introducing lens sizes as an extra parameter in the finite-source model (see Figure 12). This implies that the lens size effect is negligible for OGLE-2003-BLG-262.

6. CONCLUSION

We have demonstrated that finite-source effects can be more conveniently evaluated in the lens-centered polar coordinate system. The uniform source case can be reduced to a one-dimensional integral, which can be solved in a fast and numerically stable manner. The previously available formalisms were either comparably fast but held only in the high-amplification regime (the Gould finite-source approximation) or held in any amplification regime but involved an integral which has singularity and is slower to solve (the Witt & Mao approach). We also showed that the vast majority of the OGLE-lensing events have maximum amplifications smaller than 10, and therefore cannot be precisely described in the high-amplification, finite-source approximation of Gould. Our formalism allows a fast and simultaneous search for microlensing events with extended or pointlike sources in any amplification regime.

We also presented the limb-darkening effects and finite lens size effects in our formalism. We showed for the case of OGLE-2003-BLG-262 how one can constrain the source size and obtain upper limits for the lens size.

The Appendix provides the partial derivatives of the amplification for a uniform surface brightness source (Appendix A), a limb-darkened source (Appendix B), and a uniform surface brightness source with a finite lens (Appendix C), which are required in, e.g., the Levenberg-Marquardt algorithm to obtain microlensing light-curve fits.

We thank Johannes Koppenhöfer for fruitful discussions. This work was supported by the DFG cluster of excellence 'Origin and Structure of the Universe' (www.universe-cluster.de).

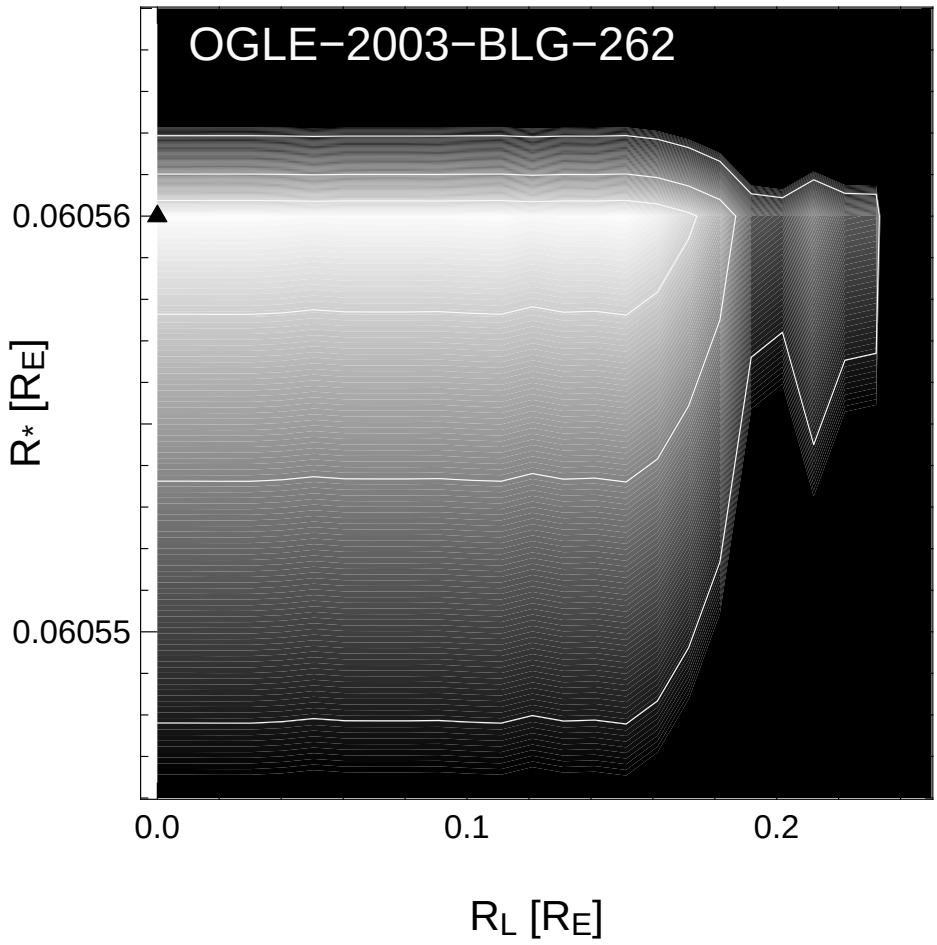

FIG. 12.— χ^2 contour map of OGLE-2003-BLG-262. In *white contour*, levels for 1, 2, and 3σ for source and lens size fitting are shown. The *black triangle* indicates the best-fitted model with $\rho = 0.06056$ and $R_{\rm lens} = 0$. This suggests that the point lens assumption is sufficient for OGLE-2003-BLG-262.

APPENDIX

A. PARTIAL DERIVATIVES OF THE FINITE-SOURCE AMPLIFICATION FOR A SOURCE WITH UNIFORM SURFACE BRIGHTNESS

$$\begin{aligned}
\frac{\partial A^*}{\partial u}(u,\rho) &= \frac{2}{\pi\rho^2}\int_0^\pi \left\{ \frac{u_2^2+2}{\sqrt{u_2^2+4}}\left[\cos\vartheta - \frac{u\sin^2\vartheta}{\sqrt{\rho^2-u^2\sin^2\vartheta}}\right] - \frac{u_1^2+2}{\sqrt{u_1^2+4}}\left[\cos\vartheta + \frac{u\sin^2\vartheta}{\sqrt{\rho^2-u^2\sin^2\vartheta}}\right]\right\} d\vartheta \\
\frac{\partial A^*}{\partial \rho}(u,\rho) &= \frac{2}{\pi\rho}\int_0^\pi \left[\frac{u_2^2+2}{\sqrt{u_2^2+4}\sqrt{\rho^2-u^2\sin^2\vartheta}} - \frac{u_1^2+2}{\sqrt{u_1^2+4}\sqrt{\rho^2-u^2\sin^2\vartheta}}\right] d\vartheta - 2\frac{A^*(u,\rho)}{\rho} \ .
\end{aligned} \tag{A1}$$

B. PARTIAL DERIVATIVES OF THE FINITE-SOURCE AMPLIFICATION FOR A SOURCE WITH LIMB DARKENING

$$\begin{aligned}
\frac{\partial A^*(u,\rho,\Gamma_\lambda)}{\partial u} &= \frac{2}{\pi\rho^2}\int_0^\pi \left[\frac{\partial u_2}{\partial u}\frac{u_2^2+2}{\sqrt{u_2^2+4}}\frac{S_\lambda}{S_\lambda} - \frac{\partial u_1}{\partial u}\frac{u_1^2+2}{\sqrt{u_1^2+4}}\frac{S_\lambda}{S_\lambda}\right] d\vartheta + \frac{2}{\pi\rho^2}\int_0^\pi\int_{u_1}^{u_2}\frac{\tilde{u}^2+2}{\sqrt{\tilde{u}^2+4}}\frac{\partial}{\partial u}\left(\frac{S_\lambda}{S_\lambda}\right) d\tilde{u}d\vartheta \\
\frac{\partial A^*(u,\rho,\Gamma_\lambda)}{\partial \rho} &= \frac{2}{\pi\rho^2}\int_0^\pi \left[\frac{\partial u_2}{\partial \rho}\frac{u_2^2+2}{\sqrt{u_2^2+4}}\frac{S_\lambda}{S_\lambda} - \frac{\partial u_1}{\partial \rho}\frac{u_1^2+2}{\sqrt{u_1^2+4}}\frac{S_\lambda}{S_\lambda}\right] d\vartheta + \frac{2}{\pi\rho^2}\int_0^\pi\int_{u_1}^{u_2}\frac{\tilde{u}^2+2}{\sqrt{\tilde{u}^2+4}}\frac{\partial}{\partial \rho}\left(\frac{S_\lambda}{S_\lambda}\right) d\tilde{u}d\vartheta - 2\frac{A^*(u,\rho,\Gamma_\lambda)}{\rho} \\
\frac{\partial A^*(u,\rho,\Gamma_\lambda)}{\partial \Gamma_\lambda} &= \frac{2}{\pi\rho^2}\int_0^\pi\int_{u_1}^{u_2}\frac{\tilde{u}^2+2}{\sqrt{\tilde{u}^2+4}}\frac{\partial}{\partial \Gamma_\lambda}\left(\frac{S_\lambda}{S_\lambda}\right) d\tilde{u}\,d\vartheta
\end{aligned} \tag{B1}$$

with $\frac{\partial u_1}{\partial u} = \cos\vartheta + u\sin^2\vartheta/\sqrt{\rho^2-u^2\sin^2\vartheta}$, $\frac{\partial u_2}{\partial u} = \cos\vartheta - u\sin^2\vartheta/\sqrt{\rho^2-u^2\sin^2\vartheta}$, $\frac{\partial u_1}{\partial \rho} = -\rho/\sqrt{\rho^2-u^2\sin^2\vartheta}$, $\frac{\partial u_2}{\partial \rho} = \rho/\sqrt{\rho^2-u^2\sin^2\vartheta}$, $\frac{\partial}{\partial u}\left(\frac{S_\lambda}{S_\lambda}\right) = -\frac{3}{4}\Gamma_\lambda(-2\tilde{u}\cos\vartheta+2u)/\left(\rho^2\sqrt{1-\frac{\tilde{u}^2-2u\tilde{u}\cos\vartheta+u^2}{\rho^2}}\right)$, $\frac{\partial}{\partial \rho}\left(\frac{S_\lambda}{S_\lambda}\right) = \frac{3}{2}\Gamma_\lambda(\tilde{u}^2-2u\tilde{u}\cos\vartheta+u^2)/\left(\rho^3\sqrt{1-\frac{\tilde{u}^2-2u\tilde{u}\cos\vartheta+u^2}{\rho^2}}\right)$, $\frac{\partial}{\partial \Gamma_\lambda}\left(\frac{S_\lambda}{S_\lambda}\right) = -1+\frac{3}{2}\sqrt{1-\frac{\tilde{u}^2-2u\tilde{u}\cos\vartheta+u^2}{\rho^2}}$ when u_1 and u_2 are not equal to zero.

C. PARTIAL DERIVATIVES OF THE FINITE-SOURCE AND FINITE-LENS AMPLIFICATION ASSUMING A SOURCE WITH UNIFORM BRIGHTNESS

$$\begin{aligned}
\frac{\partial A^*}{\partial u}(u,\rho,\rho_{\rm lens}) &= \frac{1}{\pi\rho^2}\int_0^\pi \frac{\partial u_2}{\partial u}\left[\left(A_{\rm PS}(u_2)+1\right)\Theta\left(u_2-\rho_{\rm lens}+\frac{1}{\rho_{\rm lens}}\right)+\left(A_{\rm PS}(u_2)-1\right)\Theta\left(-u_2-\rho_{\rm lens}+\frac{1}{\rho_{\rm lens}}\right)\right]u_2\,d\vartheta \\
&\quad -\frac{1}{\pi\rho^2}\int_0^\pi \frac{\partial u_1}{\partial u}\left[\left(A_{\rm PS}(u_1)+1\right)\Theta\left(u_1-\rho_{\rm lens}+\frac{1}{\rho_{\rm lens}}\right)+\left(A_{\rm PS}(u_1)-1\right)\Theta\left(-u_1-\rho_{\rm lens}+\frac{1}{\rho_{\rm lens}}\right)\right]u_1\,d\vartheta \\
\frac{\partial A^*}{\partial \rho}(u,\rho,\rho_{\rm lens}) &= \frac{1}{\pi\rho^2}\int_0^\pi \frac{\partial u_2}{\partial \rho}\left[\left(A_{\rm PS}(u_2)+1\right)\Theta\left(u_2-\rho_{\rm lens}+\frac{1}{\rho_{\rm lens}}\right)+\left(A_{\rm PS}(u_2)-1\right)\Theta\left(-u_2-\rho_{\rm lens}+\frac{1}{\rho_{\rm lens}}\right)\right]u_2\,d\vartheta \\
&\quad -\frac{1}{\pi\rho^2}\int_0^\pi \frac{\partial u_1}{\partial \rho}\left[\left(A_{\rm PS}(u_1)+1\right)\Theta\left(u_1-\rho_{\rm lens}+\frac{1}{\rho_{\rm lens}}\right)+\left(A_{\rm PS}(u_1)-1\right)\Theta\left(-u_1-\rho_{\rm lens}+\frac{1}{\rho_{\rm lens}}\right)\right]u_1\,d\vartheta \\
&\quad -2\frac{A^*(u,\rho,\rho_{\rm lens})}{\rho} \\
\frac{\partial A^*}{\partial \rho_{\rm lens}}(u,\rho,\rho_{\rm lens}) &= \frac{1}{\pi\rho^2}\int_0^\pi\int_{u_1}^{u_2}\left(A_{\rm PS}(\tilde{u})+1\right)\delta\left(\tilde{u}-\rho_{\rm lens}+\frac{1}{\rho_{\rm lens}}\right)\frac{\partial\left(\tilde{u}-\rho_{\rm lens}+\frac{1}{\rho_{\rm lens}}\right)}{\partial\rho_{\rm lens}}\tilde{u}\,d\tilde{u}\,d\vartheta \\
&\quad +\frac{1}{\pi\rho^2}\int_0^\pi\int_{u_1}^{u_2}\left(A_{\rm PS}(\tilde{u})-1\right)\delta\left(-\tilde{u}-\rho_{\rm lens}+\frac{1}{\rho_{\rm lens}}\right)\frac{\partial\left(-\tilde{u}-\rho_{\rm lens}+\frac{1}{\rho_{\rm lens}}\right)}{\partial\rho_{\rm lens}}\tilde{u}\,d\tilde{u}\,d\vartheta \ .
\end{aligned} \tag{C1}$$

The derivatives can be obtained numerically by utilizing the same approache as shown in Equation (7). We also find that for $u > \rho$, substituting integration variable ϑ with $v \equiv \frac{u}{\rho}\sin\vartheta$ gives a numerically more stable estimations of the derivatives for a uniform brightness source:

$$\begin{aligned}
\frac{\partial A^*}{\partial u}(u,\rho) &= \frac{u}{\pi\rho}\int_0^1 \frac{1}{U^3}\left[\frac{(u^2-\rho^2)(U+\Omega)-4\Omega}{\sqrt{(U+\Omega)^2+4}} - \frac{(u^2-\rho^2)(U-\Omega)+4\Omega}{\sqrt{(U-\Omega)^2+4}}\right] dv \\
\frac{\partial A^*}{\partial \rho}(u,\rho) &= \frac{1}{\pi\rho^2}\int_0^1 \frac{1}{U^3}\left[-\frac{u^2\left(u^2-\rho^2\right)(U+\Omega)-4(\Omega v^2\rho^2-U^3)}{\sqrt{(U+\Omega)^2+4}} + \frac{u^2\left(u^2-\rho^2\right)(U-\Omega)+4(\Omega v^2\rho^2+U^3)}{\sqrt{(U-\Omega)^2+4}}\right] dv
\end{aligned} \tag{C2}$$

with $U = \sqrt{u^2-v^2\rho^2}$ and $\Omega = \rho\sqrt{1-v^2}$.

REFERENCES

Agol, E. 2002: *Occultation and Microlensing*, ApJ, 579, 430

Alcock, C., Axelrod, T. S., Bennett, D. P., Cook, K. H., Park, H. S., Griest, K., Perlmutter, S., Stubbs, C. W., Freeman, K. C., Peterson, B. A. 1992: *The search for massive compact halo objects with a (semi) robotic telescope*, ASPC, 34, 193

Alcock, C., Allen, W. H., Allsman, R. A., Alves, D., Axelrod, T. S., Banks, T. S., Beaulieu, S. F., Becker, A. C., Becker, R. H., Bennett, D. P., Bond, I. A., et al. 1997: *MACHO Alert 95-30: First Real-Time Observation of Extended Source Effects in Graviational Microlensing*, ApJ, 491, 436

Cassan, A., Beaulieu, J.-P., Fouqué, P., Brillant, S., Dominik, M., Greenhill, J., Heyrovský, D., Horne, K., Jørgensen, U. G., Kubas, D., Stempels, H. C., et al. 2006: *OGLE 2004-BLG-254: a K3 III Galactic bulge giant spatially resolved by a single microlens*, A&A, 460, 277

Gould, A. 1994: *Proper motions of MACHOs*, ApJ, 421, L71

Gould, A. 1996: *Theory of Pixel Lensing*, ApJ, 470, 201+

Heyrovsky, D. & Loeb, A. 1997: *Microlensing of an Elliptical Source by a Point Mass*, ApJ, 490, 38

Heyrovský, D. 2003: *Measuring Stellar Limb Darkening by Gravitational Microlensing*, ApJ, 594, 464

Paczyński, B. 1986: *Gravitational microlensing by the galactic halo*, ApJ, 304, 1

Press, W. H., Teukolsky, S. A., Vetterling, W. T., Flannery, B. P. 2007: Numerical recipes in C++ : the art of scientific computing (3rd ed.; Cambridge: Cambridge Univ. Press)

Riffeser, A., Fliri, J., Seitz, S., & Bender, R. 2006: *Microlensing toward Crowded Fields: Theory and Applications to M31*, ApJS, 163, 225

Udalski, A., Szymanski, M., Kaluzny, J., Kubiak, M., & Mateo, M. 1992: *The Optical Gravitational Lensing Experiment*, AcA, 42, 253

Udalski, A. 2003: *The Optical Gravitational Lensing Experiment. Real Time Data Analysis Systems in the OGLE-III Survey*, Acta Astronomica, 53, 291

Witt, H. J. & Mao, S. 1994: *Can lensed stars be regarded as pointlike for microlensing by MACHOs?*, ApJ, 430, 505

Yoo, J., DePoy, D. L., Gal-Yam, A., Gaudi, B. S., Gould, A., Han, C., Lipkin, Y., Maoz, D., Ofek, E. O., Park, B.-G., Pogge, R. W., et al. 2004: *OGLE-2003-BLG-262: Finite-Source Effects from a Point-Mass Lens*, ApJ, 603, 139